Human Molecular Genetics, 2012, Vol. 21, No. 16 ***3535–3545***
doi:10.1093/hmg/dds183
Advance Access published on May 15, 2012

Cardiopulmonary dysfunction in the Osteogenesis imperfecta mouse model Aga2 and human patients are caused by bone-independent mechanisms

Frank Thiele[1,†,‡], Christian M. Cohrs[1,‡], Armando Flor[2,¶], Thomas S. Lisse[1,§], Gerhard K. H. Przemeck[1], Marion Horsch[1], Anja Schrewe[1], Valerie Gailus-Durner[1], Boris Ivandic[3], Hugo A. Katus[3], Wolfgang Wurst[4,5], Catherine Reisenberg[2], Hollis Chaney[6], Helmut Fuchs[1], Wolfgang Hans[1], Johannes Beckers[1,7], Joan C. Marini[2], and Martin Hrabé de Angelis[1,7,*]

[1]Institute of Experimental Genetics, Helmholtz Zentrum München, German Research Center for Environmental Health (GmbH), Neuherberg, Germany, [2]Bone and Extracellular Matrix Branch, National Institute of Child Health and Human Development, NIH, Bethesda, MD, USA, [3]Department of Medicine III, Division of Cardiology, University of Heidelberg, Heidelberg, Germany, [4]Institute of Developmental Genetics, Helmholtz Zentrum München, German Research Center for Environmental Health (GmbH), Neuherberg, Germany, [5]Technische Universität München, Center of Life and Food Science, Weihenstephan, Chair of Developmental Genetics, Weihenstephan, Germany, [6]Children's National Medical Center, Washington, DC, USA and [7]Technische Universität München, Center of Life and Food Science, Weihenstephan, Chair of Experimental Genetics, Weihenstephan, Germany

Received March 19, 2012; Revised and Accepted May 10, 2012

Osteogenesis imperfecta **(OI) is an inherited connective tissue disorder with skeletal dysplasia of varying severity, predominantly caused by mutations in the collagen I genes (*COL1A1*/*COL1A2*). Extraskeletal findings such as cardiac and pulmonary complications are generally considered to be significant secondary features. *Aga2*, a murine model for human OI, was systemically analyzed in the German Mouse Clinic by means of *in vivo* and *in vitro* examinations of the cardiopulmonary system, to identify novel mechanisms accounting for perinatal lethality. Pulmonary and, especially, cardiac fibroblast of perinatal lethal *Aga2*/+ animals display a strong down-regulation of *Col1a1* transcripts *in vivo* and *in vitro*, resulting in a loss of extracellular matrix integrity. In addition, dysregulated gene expression of *Nppa*, different types of collagen and *Agt* in heart and lung tissue support a bone-independent vicious cycle of heart dysfunction, including hypertrophy, loss of myocardial matrix integrity, pulmonary hypertension, pneumonia and hypoxia leading to death in *Aga2*. These murine findings are corroborated by a pediatric OI cohort study, displaying significant progressive decline in pulmonary function and restrictive pulmonary disease independent of scoliosis. Most participants show mild cardiac valvular regurgitation, independent of pulmonary and skeletal findings. Data obtained from human OI patients and the mouse model *Aga2* provide novel evidence for primary effects of type I collagen mutations on the heart and lung. The findings will have potential benefits of anticipatory clinical exams and early intervention in OI patients.**

*To whom correspondence should be addressed at: Institute of Experimental Genetics, Helmholtz Zentrum München, German Research Center for Environmental Health (GmbH), Neuherberg, Germany. Tel: +49 8931873502; Fax: +49 8931873500; Email: hrabe@helmholtz-muenchen.de
†Present Address: Institute of Virology, Klinikum Rechts der Isar, Munich, Germany.
‡The authors wish it to be known that, in their opinion, the first two authors should be regarded as joint First Authors.
¶Present Address: Wyeth Pharmaceuticals, King of Prussia, PA, USA.
§Present address: Mount Desert Island Biological Lab, Salisbury Cove, ME, USA.

INTRODUCTION

Brittle bones, fractures and osteoporosis are symptoms of *Osteogenesis imperfecta* (OI), a group of inherited connective tissue disorders. Patients are classified in nine types ranging from mild, with few fractures, to severe forms with perinatal lethality (1–3). Most OI cases are caused by autosomal dominant mutations in *COL1A1* or *COL1A2*, which encode the chains of type I collagen, the most abundant protein of the extracellular matrix (ECM) of bone (4).

Although skeletal findings are predominant, OI is a generalized connective tissue disorder as type I collagen comprises, in addition to bone, skin and tendon (5), ~80% of lung and cardiac collagen. The non-skeletal manifestations of OI in the respiratory and cardiovascular systems are responsible for most mortality and morbidity in severe and moderate types II–IV OI, but these effects have not been directly linked to the underlying collagen mutation and have been considered secondary to skeletal changes (6,7). Pulmonary complications are the leading cause of deaths in OI generally attributed to secondary effects of scoliosis or rib fractures (4,7–9), although the presence of severe restrictive lung disease with relatively small scoliosis curve raised the possibility of an intrinsic defect (8). Two case studies of lethal OI with lung hypoplasia suggested that abnormal collagen might be directly causal (10,11). Cardiovascular findings, including valvular insufficiency, aortic root dilation, atrial septal defects and septal and posterior left ventricular wall thickening have been reported in OI (12–19). Right-sided heart failure (cor pulmonale) in OI is considered a late effect of pulmonary dysfunction (7). Altered cardiac structure of heterozygous *Col1a2*-deficient *oim* mice, including increased septal and posterior wall thickness, and left ventricular volume (20), as well as decreased integrity of the thoracic aorta (21), was associated with decreased collagen and indicates the importance of the absent a2(I) chain. Collagen was also decreased and disorganized in the heart and great vessels of two OI type II fetuses (22), but direct relationship to mortality was not studied.

In the Munich ENU mutagenesis screen (23), we identified a new mouse model for OI, termed *Aga2*, with a dominant frameshift mutation in the Col1a1 C-propeptide domain (24). *Aga2* mice have OI phenotypic changes and endoplasmatic reticulum (ER) stress-related apoptosis in bone tissue (24). Two distinct phenotypes of *Aga2* can be distinguished. Mildly affected animals survive to adulthood ($Aga2^{mild}$) and make up 66% of all *Aga2*/+ mice, while other *Aga2*/+ mice ($Aga2^{severe}$) are postnatally lethal (34%) even with bisphosphonate administration. Considering the discrete *Aga2* phenotypes, resembling the hallmarks of moderate and lethal OI caused by collagen defects, we systemically phenotyped *Aga2* mice at the German Mouse Clinic (GMC). Here, we provide evidence that the *Aga2* type I collagen mutation directly causes pathological changes in heart and lung tissue that are bone-independent and are the primary cause of death in $Aga2^{severe}$.

The direct relevance of the bone-independent *Aga2* findings to pathogenic mechanisms in human OI is demonstrated by the findings presented here from a pediatric type III and IV OI longitudinal study population at the NICHD, NIH. The patients have collagen mutations causing severe and moderate non-lethal OI, corresponding more to non-lethal *Aga2* mice ($Aga2^{mild}$). Children both with and without scoliosis were shown to have clinically significant decline of pulmonary function during childhood, as well as primary cardiac valvular and chamber abnormalities.

RESULTS

Phenotypic classification of heterozygous *Aga2*

Among heterozygous *Aga2* mice, two different groups can be discerned by days 6–11 after birth (24). The first group has mild symptoms ($Aga2^{mild}$), 75% ($\pm 9.6\%$, $n = 16$) of wild-type (WT) body weight and survives to adulthood. The second group contains severely affected mutants ($Aga2^{severe}$), which have a substantial reduction in body weight to 53% ($\pm 3.9\%$, $n = 12$) of wild-type littermates and succumb to postnatal lethality. The post-natal lethality of $Aga2^{severe}$ mice was not altered in response to treatment with the bisphosphonate alendronate compared with controls (Supplementary Material, Fig. S1). Transmission electron microscopy (TEM) analysis of cellular alterations shows disordered cytoplasm and changes in ER and Golgi in $Aga2^{severe}$ cardiac fibroblasts (Supplementary Material, Fig. S2). The upregulation of apoptotic markers demonstrated in *Aga2* osteoblasts (24) was not detected and was regarding *Hspa5* and *Serpinh1* by trend even downregulated in heart and lung tissue (Supplementary Material, Fig. S2).

Aga2 cardiovascular function and histology

Despite the markedly decreased body weight, $Aga2^{severe}$ hearts possessed enlarged septa and right ventricular hypertrophy (Fig. 1A). In contrast to type I collagen immunohistochemical staining on heterozygous $Col1a1^{Mov13}$ mice (25) showing reduced staining due to haploinsufficiency, $Aga2^{severe}$ revealed an altered staining pattern in addition to reduced collagen amount in the myocardium (Fig. 1B). Scanning electron microscopy (SEM) analysis confirmed that $Aga2^{severe}$ mice have disordered matrix collagen in cardiac tissue (Fig. 1C), with fewer and thinner collagen fibrils. Platelet endothelial cell adhesion molecule (PECAM) antibody staining was reduced in vascular endothelium, and also revealed disordered cell arrangements and thinner walls, implying defective blood vessel integrity in $Aga2^{severe}$ hearts (Fig. 1D).

While hearts of $Aga2^{severe}$ mice had normal maximum extension during diastole in ultrasound analysis, left ventricular end-systolic internal diameter (LVESD) was significantly higher (Fig. 1E), resulting in a significantly lower ejection fraction (EF), suggesting an impaired muscle contraction. In addition, the B-mode analysis of $Aga2^{severe}$ mice revealed septal deformation with a convex bulge into the left ventricle during contraction (Supplementary Material, Video S1). In $Aga2^{mild}$, electrocardiogram (ECG) revealed an extended J-T interval and increased QRS amplitude with normal echocardiograms.

In vitro analysis of cardiac cell function and gene expression analysis

Immunocytochemistry on cardiac fibroblasts displayed a strong reduction in type I collagen staining in both $Aga2^{severe}$

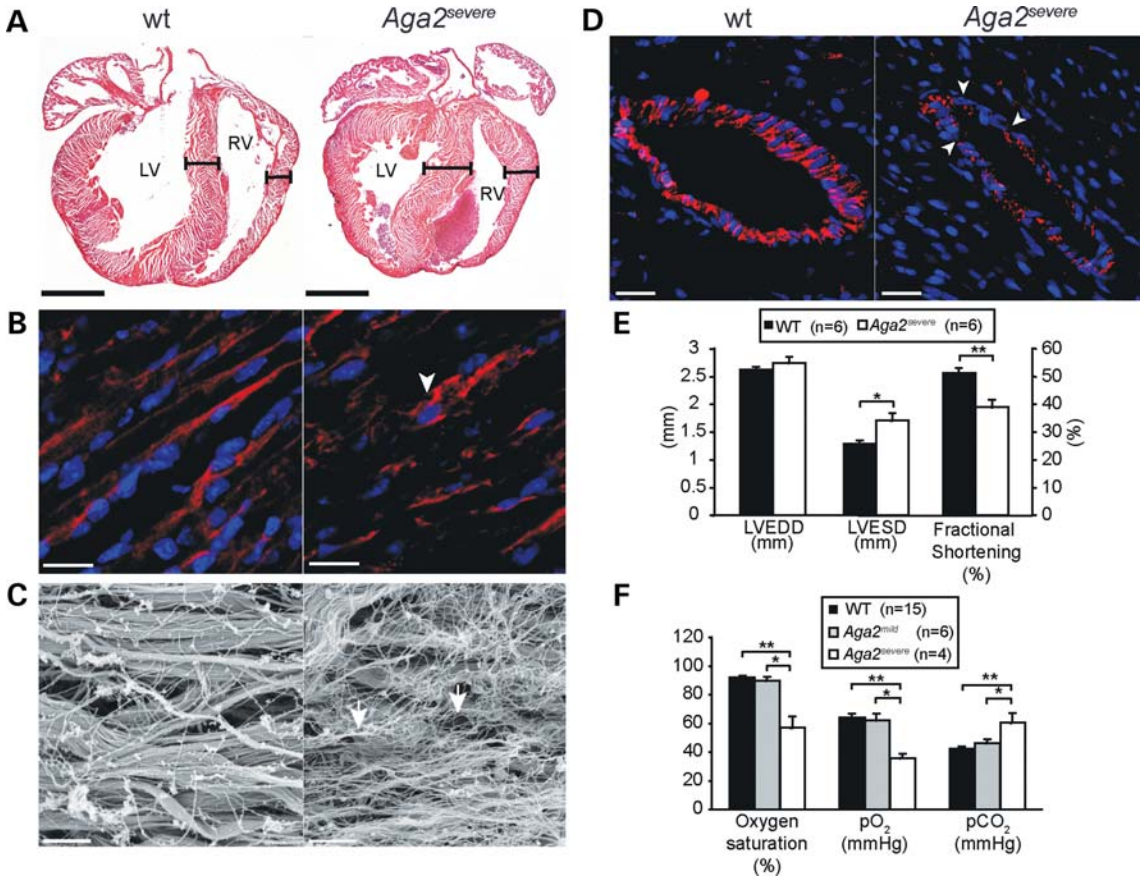

Figure 1. *In vivo* cardiac findings. (**A**) H&E staining of longitudinal heart sections of WT and *Aga2*^{severe}. Black bars indicate enlarged septum and right ventricular hypertrophy. (**B**) Immunohistological staining of type I collagen in hearts of WT and *Aga2*^{severe}. Arrowhead shows type I collagen accumulation close to the nuclei. (**C**) SEM of the myocard. Arrows indicate increased content of smaller collagen fibers. (**D**) Immunohistochemical staining of PECAM for morphological analysis of blood vessels in the myocard. Arrowheads show loss of cell arrangement and reduced PECAM staining. (**E**) Echocardiographic data from WT and *Aga2*^{severe} hearts. (**F**) Blood gas analysis of WT, *Aga2*^{mild} and *Aga2*^{severe}. LV, left ventricle; RV, right ventricle; Scale bars in (C) and (D) = 1 mm; (E) and (F) = 10 μm; (G) and (H) = 3 μm; (I) and (J) = 20 μm. $^{*}P \leq 0.05$, $^{**}P \leq 0.01$.

cells and ECM (Fig. 2A), and a slight decrease in collagen staining in *Aga2*^{mild} cells. Quantitative real-time PCR (qRT–PCR) for *Col1a1* verified reduction in transcript expression to 25 and 65% of WT levels in *Aga2*^{severe} and *Aga2*^{mild} cardiac fibroblasts, respectively (Fig. 2C).

In *Aga2*^{severe} heart tissue, genome-wide transcriptome analysis identified 48 significantly differentially expressed genes, compared with WT animals, also partially verified via qRT–PCR (Supplementary Material, Fig. S3). Gene Ontology (GO) term analysis (Supplementary Material, Table S1) of differentially expressed genes revealed an association with the composition and remodeling of ECM. Strikingly, *Col1a1* was the most prominently regulated gene, showing a 2.5-fold downregulation in *Aga2*^{severe}, confirmed by 4-fold *Col1a1* repression compared with WT by qRT–PCR (Fig. 2D). In addition, *Col1a2, Col2a1* and *Col3a1* expression as well as key factors of collagen fibrillogenesis and matrix assembly (*Dpt, Mfap4*) were downregulated. Upregulation of *Col8a1*, *Tgm2* and *Ctgf* indicated pronounced ECM remodeling. Changes in metabolic pathways and alteration of oxygen supply were suggested by upregulation of *Egln3*, *Ldha*, *Aldoa*, *Eno1*, *Gapdh* and *Pgm2*, indicating hypoxia. Consistent with the histological examinations, markers for hypertrophy (*Nppa, Slc25a4*) were upregulated.

Onset of *Col1a1* downregulation and analysis of allele-specific *Col1a1* expression in the heart

Given the strong reduction in collagen transcripts and protein in the hearts of *Aga2*^{severe} animals, we examined *Col1a1* expression in heart tissue during *Aga2* etiology [14 and 20 days post-coitum (dpc), and 1, 3 and 6 days *post-partum* (dpp)]. Remarkably, *Col1a1* expression was decreased consistently until 3 dpp in all heterozygous animals to 55–70% of WT littermates (Fig. 2E). At 6 dpp, the first *Aga2*^{severe} mouse was evident, with *Col1a1* downregulation to 25% of control. Although only one animal was discernable at this age, the values were equal to the results in older animals (Fig. 2C).

To further substantiate the difference in type I collagen expression in mutant mice, allele-specific *Col1a1* expression was analyzed. In 14 dpc to 6 day-old mice without distinguishable phenotypes, expression of the WT allele (*Col1a1*^{WT}) in *Aga2* was 50–60%, while the mutated allele (*Col1a1*^{Aga2}) was

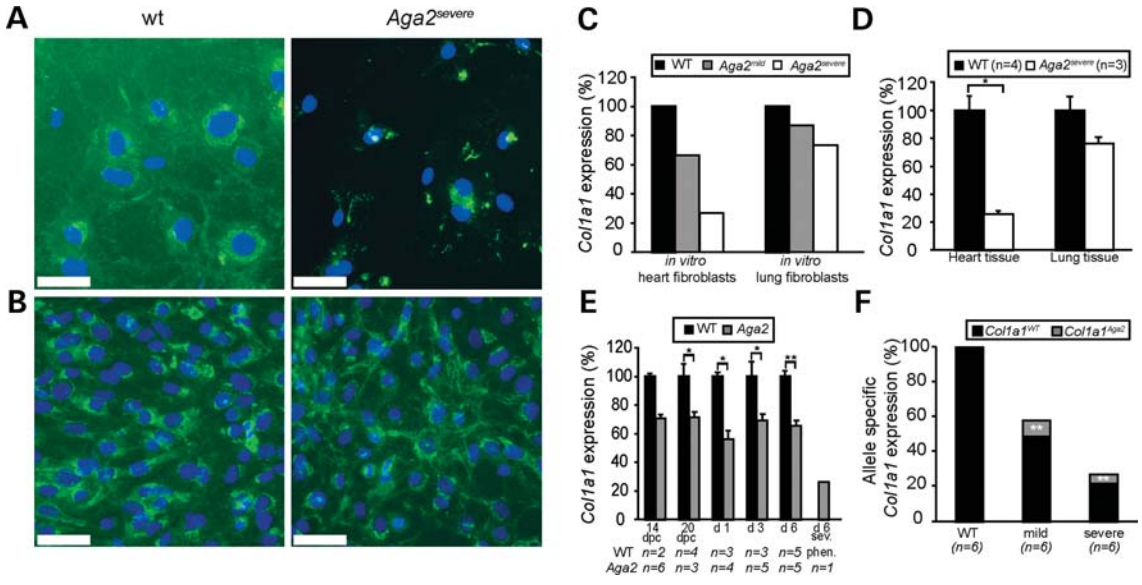

Figure 2. *In vitro* culture of primary heart and lung fibroblasts and expression analysis by qRT–PCR. (**A** and **B**) ICC for type I collagen (green) on heart fibroblasts (A) and lung fibroblasts (B) counterstained with DAPI (blue). (**C**) Overall *Col1a1* expression of *in vitro* cultivated primary heart and lung fibroblasts ($n = 3$ for each group, pooled). (**D**) Overall *Col1a1* expression in heart and lung tissue. (**E**) Overall *Col1a1* expression in hearts during embryonic and perinatal stages (14 dpc–6 dpp). (**F**) Allele-specific *Col1a1* expression in hearts of $Aga2^{mild}$ and $Aga2^{severe}$ at 10–11 dpp. Statistics were performed assuming the $Col1a1^{WT}$ allele is only expressed to 50% in WT mice (corresponding to a single gene copy). Scale bars in (A and B) = 100 μm; (C and D) = 200 μm; $^{*}P \leq 0.05$, $^{**}P \leq 0.01$.

strongly repressed to ~10% (Supplementary Material, Fig. S4). These data imply normal transcription of the $Col1a1^{WT}$ allele and reduced transcription of $Col1a1^{Aga2}$ in mutant mice, consistent with the *in vitro* data of $Aga2^{mild}$ (Fig. 2C). Investigation for a potential nonsense-mediated decay of the mutant allele was performed by emetine treatment *in vitro* using lung fibroblasts. As expected, emetine treatment was able to restore the $Col1a1^{Aga2}$ allele, while $Col1a1^{WT}$ was unaffected by treatment (Supplementary Material, Fig. S5).

Allele-specific collagen expression analysis of 10–11 dpp mice with distinctive $Aga2^{mild}$ and $Aga2^{severe}$ phenotypes was performed to confirm and statistically evaluate the findings of 6-day-old *Aga2* mice (Fig. 2F). Results revealed that $Aga2^{mild}$ animals expressed the $Col1a1^{WT}$ allele to 50% and the mutated $Col1a1^{Aga2}$ allele to 10% compared with the $Col1a1^{WT}$ allele in the littermates, thus resembling the data obtained from younger animals. Strikingly, in hearts of $Aga2^{severe}$ mice, a strong downregulation of the $Col1a1^{WT}$ allele to 20% and a reduction in $Col1a1^{Aga2}$ to 5% suggested further silencing of collagen expression in hearts of severe mutants.

Cardiac findings in children with types III and IV OI

To further substantiate our findings in *Aga2*, 46 children and young adults [aged 3–23 years (mean 12 ± 4.2)] with types III (progressive deforming) and IV (moderately severe) OI, most with known collagen mutations, underwent echocardiogram and ECG. In both groups, 78% (18/23) of participants had one or more valvular or cardiac chamber findings (Table 1). Mild tricuspid regurgitation was the most common finding, and occurred in over half of participants with each type. Two type III and 10 type IV patients had combined mild mitral, pulmonic or aortic regurgitation in addition to the tricuspid valve finding. Only two participants, both type III, had mitral regurgitation without a concurrent pulmonic valve finding. Small intracardiac shunts were detected in three type III OI participants who also had pulmonic valve regurgitation and all mild left-to-right flows across an atrial septal defect. Mild left atrial enlargement was reported in two type III [one also with premature atrial contractions (PACs)] and three type IV OI patients. Seven participants had ECG findings, including five type III OI patients with sinus tachycardia, sinus tachycardia with Q waves, high right ventricular voltage, low voltage in PR or PACs, and two type IV OI patients with PACs or sinus arrhythmia and high left ventricular voltage.

Aga2 pulmonary findings

Lungs of $Aga2^{severe}$ and $Aga2^{mild}$ mice were compared with WT littermates. While $Aga2^{mild}$ lungs appeared morphologically normal, $Aga2^{severe}$ lungs were hemorrhagic with alveolar bleeding throughout the tissue, and infiltrated with polymorphonuclear neutrophils and alveolar macrophages (Fig. 3A). Since rib fractures with callus formation were equally frequent in $Aga2^{mild}$ and $Aga2^{severe}$ animals, lung hemorrhages of $Aga2^{severe}$ mice could not be explained by fractures (Fig. 3B). PECAM antibody staining of lung vasculature (Fig. 3C) displayed marginal reduction in staining in $Aga2^{mild}$, while capillary staining in hemorrhages of $Aga2^{severe}$ was strongly diminished and visible only where alveoli were not hemorrhagic.

Blood gas analysis revealed a reduction of 44% in arterial pO_2 and an increase of 40% in pCO_2 only in $Aga2^{severe}$

Table 1. Data on the examined type III and IV OI patients

ID	Type	Mutation	Age	Echocardiogram						PFT		Spine	Pam
				T	M	P	A	LV	LA	Restr	Obstr		
1	IV	α1 (I) p.(Gly266Glu)	17–23	+	MVP	+/I	+/I	–	–	+	–	15–25	
2	IV	α1 (I) p.(Gly1022Ala)	12	+	+	+	–	–	–	+	–	10	+
3	IV	α1 (I) p.(Gly191Asp)	9–13	+	+	–	+	–		++	–	10–40	+
4	IV	α1 (I) p.(Gly530Ser)	13–19	+	+	–	–	–	–	+	–	25–40	
5	IV	Unknown	12–16	+	+	–	–	–	DIL	–	+	25–45	
6	IV	α1 (I) p.(Gly767Ser)	10–14	+	+	–	–	–		++	–	40–60	
7	IV	α2 (I) p.(Gly334Ser)	8–10	+	+	–	–	–		+	–	15	+
8	IV	α1 (I) p.(Gly626Ser)	5–8	+	+	–	–	–	–	–	–	15–30	+
9	IV	α2 (I) p.(Gly601Ser)	10–17	+	–	+	–	–		–	–	15–20	+
10	IV	α2 (I) p.(Gly1012Ser)	10–17	+	–	–	+	–	–	+++	–	10–15	
11	IV	Unknown	5–7	+	–	–	–	–		–	–	10–15	
12	IV	α2 (I) p.(Gly328Ser)	9–11	+	–	–	–	–		–	+	10	+
13	IV	Unknown	10–13	+	–	–	–	–		+	–	15	+
14	IV	α2 (I) p.(Gly328Ser)	7–12	+	–	–	–	–		+	–	10–20	+
15	IV	α2 (I) p.(Gly211Asp)	4	+	–	–	–	–				0	
16	IV	α2 (I) Δ E16	7–11	+	–	–	–	–				15–20	+
17	IV	α1 (I) p.(Thr1298Ile)	16	–	–	–	–	–		+++	–	10	
18	IV	α1 (I) p.(Gly701Cys)	18–21	–	–	–	–	–		++	–	30–45	
19	IV	α2 (I) p.(Gly358Ser)	16–19	–	–	–	–	–		++	–	40–55	
20	IV	α2 (I) p.(Gly328Ser)	3–9	–	–	–	–	–		–	–	0	+
21	IV	α1 (I) p.(Gly314Arg)	14	–	–	–	–	–		–	–	0–10	
22	IV	α1 (I) p.(Pro1444His)	7–9	–	–	–	–	–	DIL	–	+	10	
23	IV	α1 (I) p.(Gly767Ser)	16	–	–	–	–	–	DIL	+	–	42	
24	III	α1 (I) p.(Gly365Ala)	4–8	+	+	+	–	–	–	+	+	10–45	+
25	III	α2 (I) p.(Gly196Val)	11	+	+	–	–	–	DIL	–	–	0	
26	III	α1 (I) p.(Gly395Ser)	6–8	+	–	–	–	–		+	+	10–20	+
27	III	Unknown	7–8	+	–	–	–	–		++	–	15	
28	III	α2 (I) p.(Gly337Cys)	15–20	+	–	–	–	–		+++	–	60–70	
29	III	α2 (I) p.(Gly427Ser)	10–14	+	–	–	–	–	–	–	–	15–35	+
30	III	Unknown	12–16	+	–	–	–	–		–	+	10–25	
31	III	α1 (I) p.(Gly1076Ser)	4–7	+	–	–	–	–	–	+	–	0–30	+
32	III	α1 (I) Δ E41	5	+	–	–	–	–		–	–	15	
33	III	α2 (I) p.(Gly793Arg)	6–8	+	–	–	–	–		–	–	10–20	
34	III	Unknown	11–13	+	–	–	–	–	L>R	++	–	20–25	
35	III	α1 (I) p.(Gly332Arg)	9–12	+	–	–	–	–		++	–	35–55	+
36	III	α1 (I) p.(Gly371Ser)	7–12	+	–	–	–	–		+	++	20–70	+
37	III	α1 (I) p.(Gly293Val)	12–17	+	–	–	–	–	L>R	++	++	40–50	
38	III	α2 (I) p.(Gly988Val)	12–18	+	–	–	–	–	L>R	+++	–	0–50	
39	III	α1 (I) p.(Gly254Glu)	12–13	–	++	–	–	–		++	–	25–35	+
40	III	α1 (I) p.(Gly1175Ser)	4–6	–	+	–	–	–	–	–	–	0	+
41	III	α1 (I) p.(Gly464Arg)	12	––	–	–	–			–	++	20	+
42	III	α2 (I) p.(Gly460Ser)	14	–	–	–	–	–	DIL	–	–	55	
43	III	α1 (I) p.(Gly410Ser)	7	–	–	–	–			–	–	20	+
44	III	α1 (I) Δ E33–36	11–16	–	–	–	–			+	–	30–70	
45	III	α1 (I) p.(Gly767Ser)	5–10	–	–	–	–	–		–	+	0	+
46	III	α2 (I) p.(Gly340Ser)	9–14	–	–	–	–	–	–	++++	–	20–50	

ID, patient identification number; Type, OI type; Age, age range during serial testing; T, tricuspid valve; M, mitral valve; A, aortic valve; P, pulmonic valve (+, mild regurgitation; ++, moderate regurgitation; MVP, mitral valve prolapse; I, insufficiency; –, normal). LV, left ventricle; LA, left atrium (DIL, dilated; L>R, left to right shunt; –, normal). Restr, restrictive lung disease; Obstr, obstructive lung disease (+, mild; ++, moderate; +++, severe; ++++, very severe ; –, normal). Spine, degrees of curvation; Pam, pamidronate (+, received during testing period).

compared with WT littermates (Fig. 1F). This was accompanied by a 61% decrease in oxygen saturation, suggesting hypoxic conditions due to gas exchange deficits.

In vitro analysis of lung cell function and gene expression

In cultures of primary lung fibroblasts, type I collagen immunocytochemical staining was marginally decreased in *Aga2*^{severe} (Fig. 2B), coinciding with slightly decreased (75%) *Aga2*^{severe} *Col1a1* transcripts (Fig. 2C) also observed *in vivo* (Fig. 2D). Expression profiling of *Aga2*^{severe} lungs revealed reproducible and significant regulation of 149 genes (Supplementary Material, Fig. S6). The profile of lung ECM-related transcripts differed from that of cardiac tissue: C*ol3a1, Col5a1, Mfap2, Tnc and Dpt* were upregulated, while *Ctgf* was downregulated. Markers for inflammation and wound healing, *Wnt11*, *Tgfbi* and *Ltbp3,* showed increased expression*,* as did hypoxia markers, such as *Pltp*, *Cd248*, *AR*, *Gdf10* and *Prkce* based on GO term analysis (Supplementary Material, Table S2). The pro-angiogenic markers *Ang* and *Cxcl12* were downregulated, while upregulation of *Agt* supported hypertension.

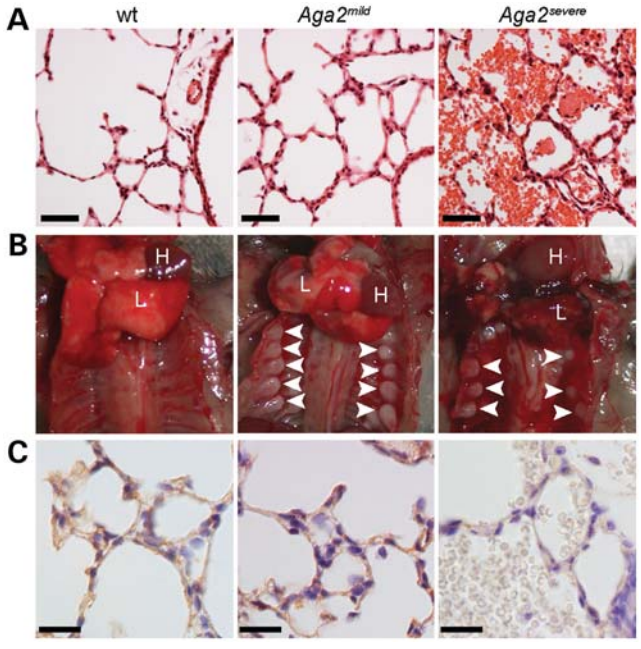

Figure 3. Histological analysis of lung tissue in *Aga2*^{mild} and *Aga2*^{severe}. (**A**) H&E staining of transversal sections of WT, *Aga2*^{mild} and *Aga2*^{severe}. (**B**) Macroscopical aspects of the thorax of WT, *Aga2*^{mild} and *Aga2*^{severe}. White arrowheads indicate callus formation at the ribs. (**C**) PECAM staining on lung tissue of WT, *Aga2*^{mild} and *Aga2*^{severe}. H, heart; L, lung; scale bars in (A) = 100 μm; (C) = 50 μm.

Pulmonary findings in children with types III and IV OI

Thirty six of 46 children and young adults in the study group (78.3%) developed scoliosis greater than 10°, with mean curvature ≈25° (range 0–70°), 10 of whom required spinal instrumentation to stabilize curve progression. OI patients with scoliosis have progressive decline of forced vital capacity (FVC), tidal lung capacity (TLC) and vital capacity (VC) with worsening scoliosis (Supplementary Material, Fig. S7), in agreement with prior studies. Pulmonary function parameters drop abruptly in patients after 30° of curvature; thereafter, the decline is gradual.

Pulmonary function parameters decline significantly with age for all OI patients, including lung volumes and flow rates (FVC: $r = -0.5$, $P < 0.001$; VC: $r = -0.5$, $P < 0.001$; TLC: $r = -0.5$, $P < 0.001$), from nearly normal at age 4 to about half of predicted values by age 20 years compared with height-matched healthy children (Fig. 4A–C). All but two participants who had three or more pulmonary function tests (PFTs) had a progressive decline of percent predicted FVC over time. The decline in FVC, TLC and VC with age was significantly greater for type III than the milder type IV OI patients.

Although scoliosis contributes to PFT decline in OI, significant decline occurs in the absence of scoliosis (Fig. 4D–F). Lung function declined significantly in 20 participants who had minimal scoliosis (≤10° curvature) at one or more time points during the study ($P = 0.008$) to ∼60% of values of younger patients. All of the participants who had significant lower airway obstruction had more severe scoliosis. Those with mild scoliosis had restrictive disease but no significant obstructive disease.

DISCUSSION

Although *Osteogenesis imperfecta* is primarily described as a bone disorder, the majority of OI mortality and morbidity is caused by respiratory and cardiac conditions, which are generally considered secondary to skeletal deformities (5,7). A primary role of the mutant collagen in cardiorespiratory disease has been suggested, but a causal connection between mutant protein and tissue pathology has not been demonstrated (4,5,7,8). As the bisphosphonate application reduced fractures, but had no effect on the survival rate of *Aga2* mice, we examined the cardiac and pulmonary tissues in heterozygous *Aga2* OI mice to unravel possible primary non-skeletal defects and their molecular mechanisms, which may underlie early lethality in OI.

In hearts and primary cardiac fibroblasts of *Aga2*^{severe} mutant mice, we observed primary structural and intrinsic cellular defects, including a strong reduction in mutant transcripts and interestingly also the WT *Col1a1* allele. While non sense-mediated decay prevents translation of the mutant allele, the WT allele has to be downregulated by other mechanisms. Since Mt1, a known positive regulator of NFkappaB (26), was strongly upregulated and NFkappaB is capable to repress *Col1a1* as well as *Col1a2* expression (27), the downregulation of both genes in *Aga2*^{severe} hearts suggests an Mt1-NFkappaB-induced downregulation of type I collagen. *Col3a1*, the minor fibrillar collagen forming heterotypic fibrils with type I collagen, as well as *Dpt* and *Mfap4*, two important proteins for collagen fibrillogenesis and matrix assembly (28,29), were also downregulated. The coordinated downregulation of these matrix molecules, in combination with mutant type I collagen heterotrimers, is likely to be the basis of collagen protein reduction and disordered spatial arrangement of collagen fibrils seen in *Aga2*^{severe} cardiac tissue. A normal collagen scaffold is needed for proper attachment and orientation of myocytes, confers myocardial stiffness and is required for adequate ventricular function (30). Thus, collagen matrix abnormalities in *Aga2*^{severe} mutant mice may lead directly to enlarged septa, right ventricular hypertrophy and impaired cardiac mechanics observed in the ultrasound analysis. This was further supported by transcriptional upregulation of *Nppa*, secreted by heart cells in response to stress and atrial stretch to modulate cardiac growth and hypertrophy (31), *Tgm2*, which increases in the transition to heart failure (32), and *Slc25a4*, involved in cardioprotection of failing hearts (33).

The lungs of *Aga2*^{severe} mice have fracture-independent hemorrhage and inflammation throughout the tissue. Capillary PECAM staining was strongly diminished although the quantity of type I collagen was normal. Upregulation of angiotensinogen and downregulated pro-angiogenic transcripts in lung tissue suggest hypertension and defects in tissue angiogenesis (34–36). Another upregulated lung ECM molecule was tenascin C (*Tnc*). It has been shown that denatured collagen increases the activity of the *Tnc* promoter (37). Therefore, although the quantity of type I collagen is only marginally changed in the lungs, structural alterations in mutated collagen may induce the *Tnc* promoter. The pathological alterations lead to hypoxemic conditions, confirmed by blood gas analysis and upregulation of hypoxic markers in the lung and heart.

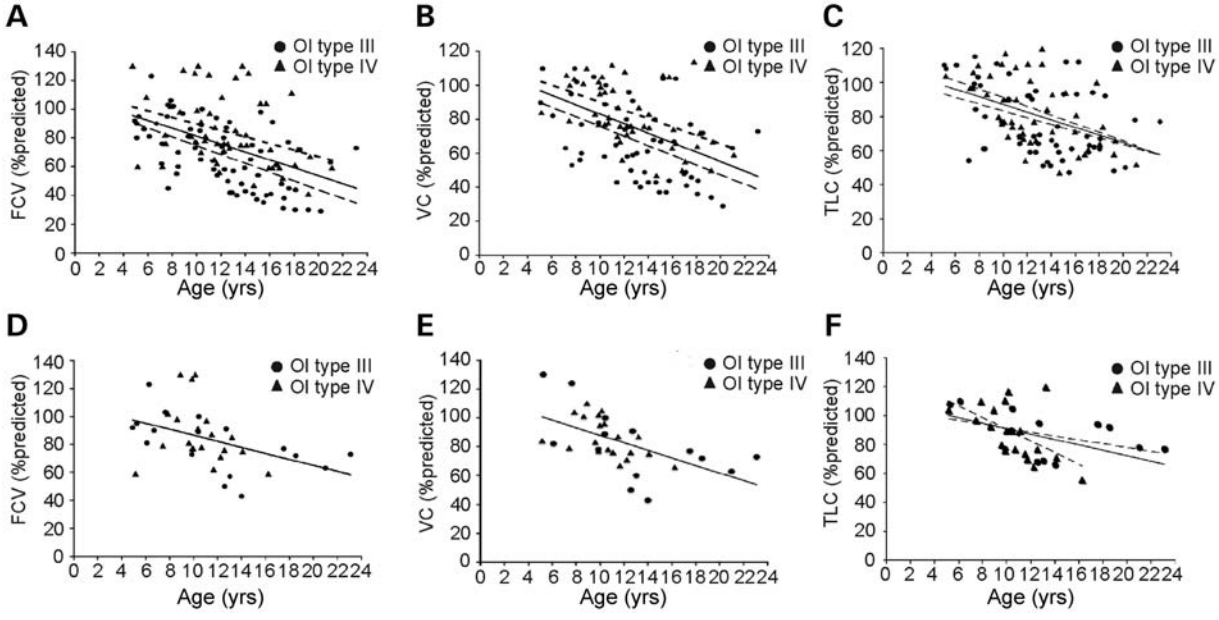

Figure 4. Relationship of age to lung volume and function in type III and IV OI patients. Lung volume and function declines in childhood in the patient cohort as a whole, as well as in types III and IV OI patients considered separately. Pulmonary function also declined significantly in children with types III and IV OI who have less than 10° scoliosis. (**A–C**) PFT results on all children in study population. (**D–F**) PFT results on children with less than 10° scoliosis. (A and D) FVC (% predicted), (B and E) VC (% predicted) and (C and F) total lung capacity (% predicted). The regression lines for the total population (solid line), type III OI (long hatch line) and type IV OI (short hatch line) are shown. Data on the Y-axis are height-normalized in (A–F).

Consequently, since both the heart and lung in *Aga2*^{severe} mice exhibit primary defects, we propose that a vicious cycle of cardiac hypertrophy and failure, pulmonary hypertension and hypoxia leads to early death (Fig. 5). In contrast to triple helical (core protein) mutations commonly found in human patients, the C-propeptide mutation in *Aga2* might not fully resemble the main human OI cases. However, the *Aga2* mouse model opens up novel opportunities in studying the etiology in particular of type III OI. Further investigation, also on the potential involvement of the NfkappaB signaling pathway, is required to clarify the basis of the pathological cycle in *Aga2*^{severe} and to determine the extent to which it models the situation in lethal forms of OI.

Aga2^{mild} is an appropriate model for non-lethal forms of OI, with moderate reduction in body size and survival to adulthood. *Aga2*^{mild} mice have moderately reduced collagen transcripts and protein staining in primary cardiac fibroblasts and marginal changes on TEM. Blood gas parameters, lung morphology and collagen protein levels are normal, with only slight reduction in PECAM staining.

The pulmonary and cardiac findings in children with non-lethal types III and IV OI due to abnormal collagen structure support the interpretation that the findings in *Aga2*^{mild} mice correlate to pre-adult development in humans. The type III and IV OI children with documented structural abnormalities of type I collagen have significant abnormalities in pulmonary function which are independent of functional cardiac abnormalities. Significant decline in tidal lung capacity and FVC occurs during childhood in OI children without scoliosis, although at a slower rate than those with more than 30° curvature. These data indicate a primary lung tissue dysfunction and also corroborates the known worsening of OI lung function with scoliosis (8,9). More than half of OI children studied have restrictive lung disease; many of those with moderate or greater severity do not have advanced scoliosis. About 20% of children studied have mild-to-moderate obstructive findings with or without restrictive disease.

Valvular regurgitation was documented in a study of OI adults with types I, IV and III OI (38), 95% of whom have combinations of tricuspid, mitral and aortic valvular regurgitation. Cardiac abnormalities in OI appear to begin in childhood for children with collagen structural abnormalities, although cardiopulmonary function at rest was normal in children with type I OI, who have reduced levels of normal collagen (39). Most (70%) of our study population had valvular regurgitation, almost all involving mild tricuspid regurgitation with about one-third of these children also having mild mitral regurgitation. Pediatric tricuspid regurgitation is likely to be related to annular dilation of primary origin, as it occurs without heart failure or elevated pulmonary artery pressures. While five children had dilated left atria and three had atrial shunting on echocardiography, five of these children had no or minimal functional lung abnormality. The follow-up of this longitudinal patient population will be required for progression of findings and contribution to OI morbidity and mortality.

Although limitations exist, based on the C-propeptide mutation in *Aga2* and the lack of human samples from lethal type III OI, the data provided here are the first report to our knowledge, which unraveled a bone-independent mechanism caused by the underlying *Col1a1* mutation in the cardiopulmonary system, leading to death in the OI model *Aga2*. While the precise molecular mechanism has still to be elucidated, the combination of murine and pediatric OI data should make

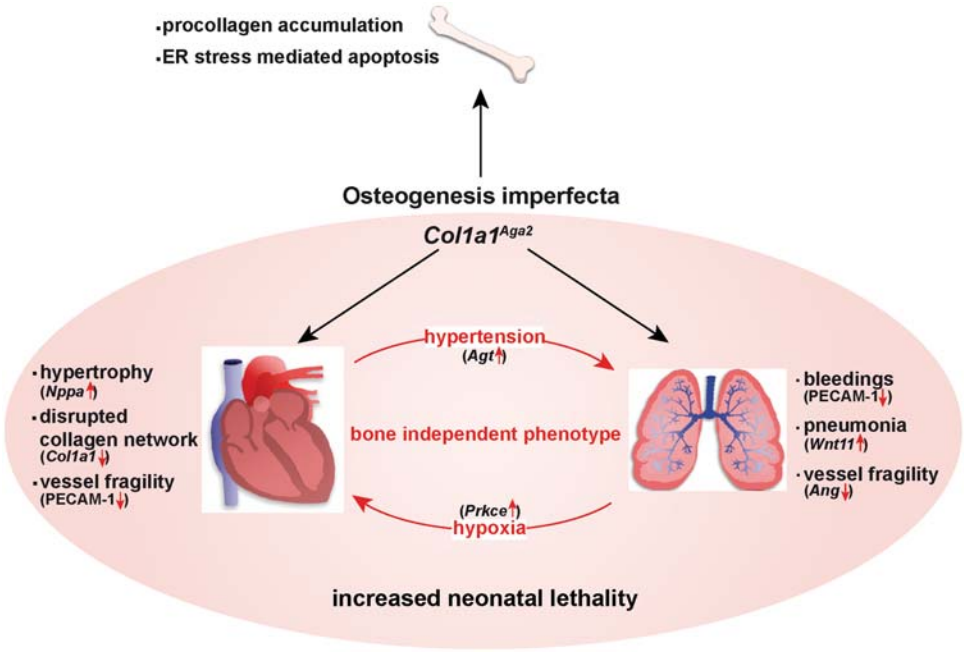

Figure 5. Schematic representation of the pathological processes provoked by the collagen mutation in *Aga2*. In bone, the expression of $Col1a1^{Aga2}$ leads to accumulation of malformed procollagen in the ER that causes the induction of UPR and triggers apoptosis. The bone-independent phenotype is caused by down-regulation of *Col1a1* in cardiac fibroblasts leading to a disrupted collagen network, accompanied with hypertrophy and vessel fragility. Cardiac alterations cause a vicious cycle of hypertension in the heart, followed by bleedings and hypoxia in the lung leading to cor pulmonale in $Aga2^{severe}$ mice.

clinicians more attentive to extra-skeletal examination of OI patients and to preventive measures such as pulmonary exercise or early evaluation for nocturnal hypoxemia. Additional murine studies on pathological mechanisms may provide insights for novel therapeutic approaches.

MATERIALS AND METHODS

Animal housing and handling

The *Aga2* mutant line was isolated from the Munich ENU mutagenesis screen conducted on the inbred strain C3HeB/FeJ (23,24), and maintained by continuing *Aga2*/+ × WT C3HeB/FeJ breedings.

Mouse husbandry was conducted under specific pathogen-free conditions in compliance with the Federation of European Laboratory Animal Science Associations protocols. Mice received standard rodent nutrition and water *ad libitum* and all animal experiments were performed under the approval of the responsible animal welfare authority. Genotyping was performed as previously described (24).

Patient population and study design

The data on children with types III and IV OI, with the follow-up into young adulthood, were obtained as part of an NICHD IRB-approved longitudinal natural history protocol (97-CH-0064) with informed parental consent. The participants included 23 with type III OI (11 boys, 12 girls; mean age 11.9 years, range 4–20 years) and 23 with type IV OI (8 boys, 15 girls; mean age 12.1 years, range 3–23 years). The type I collagen mutation has been identified in 40/46 participants. Participants have PFT at Children's National Medical Center (evaluated by HC) and cardiac evaluations at the NIH Clinical Center every 1–2 years. Data were analyzed from 46 patients who had serial examinations, comprising both longitudinal and cross-sectional data. PFTs were performed with a SensorMedic Vmax 229 analyzer®. FVC, VC and tidal lung capacity (TLC) were expressed as a percentage of predicted normal. Scoliosis was measured as Cobb angle on AP spine radiographs. For PFT parameters, multiple regression analysis was performed with the PFT measurement as the response variable, and age and scoliosis as the regressor variables. Predicted normal values and the PFT measurements were corrected for height age instead of chronological age, obtained by using the arm span, thus eliminating growth failure commonly observed for OI patients. Participants' cardiac function was evaluated with 12 lead ECG and 2D echocardiograms including spectral Doppler and M-mode assessments using commercially available machines (HP Sonos 5500 Ultrasound Cardiac Vascular®, Philips iE33 Echocardiograph®, GE Healthcare Vivid *i*® and Vivid 7 Dimension®).

Bisphosphonate treatment

To examine the effects of alendronate on the bone phenotype in *Aga2* animals, heterozygous offspring ($n = 36$) and WT littermates ($n = 44$) were each randomized in two subgroups. Starting at day 3 postnatal, the treatment group received a weekly dose of 0.03 mg/kg alendronate sodium trihydrate (Sigma, Germany) distributed on 3 s.c. injections (0.01 mg/kg/injection). The control group obtained saline in equal volume of 0.1 ml/10 g body weight. Survival analysis was

performed throughout the whole period of treatment relating the deceased animals to the survivor in each subgroup. With a smaller subset of animals ($n = 8$ for each subgroup), we continued a long time study. After 14 weeks of age, treatment was completed and DEXA and X-ray analysis was performed as previously described to assess bone parameters and fracture rate (40).

pO_2 measurement

Blood samples were collected from decapitated mice at the age of 8–11 days. Blood from the carotid artery was filled in an 85 µl blood gas capillary (Kabe, Germany). pO_2 and pCO_2 were determined by direct measurement using an ABL5 blood gas analyzer (Radiometer, Germany) and the corresponding O_2 saturation was automatically calculated.

Cardiovascular phenotyping

Heart function was investigated in *Aga2*^{mild} and WT mice at the age of 14 weeks ($n = 10$ per genotype) within the primary cardiovascular screen of the GMC (41). The assessment of the left ventricular function as secondary phenotyping was performed in 10 or 11 days old *Aga2*^{severe} mice and WT mice ($n = 6$ per genotype) by transthoracic echocardiography using high-frequency ultrasound biomicroscopy with a 30 MHz transducer and 30 Hz frame rate (Vevo 660, VisualSonics, Toronto, Canada). The shaved and anesthetized mice (1% isoflurane, Baxter, Munich, Germany) were carefully fixed in semi-supine position supported by tamponade due to brittleness of the bones. Body temperature was maintained at 36–38°C, monitored via a rectal thermometer (Indus Instruments, Houston, TX, USA). We performed four recordings and averaged the measurements from four cardiac cycles of each record for the left ventricular end-diastolic internal diameter (LVEDD) and the LVESD using the leading-edge convention, as suggested by the American Society of Echocardiography (42). Fractional shortening was calculated as FS (%) = [(LVEDD − LVESD)/LVEDD] × 100 and ejection fraction as EF (%) = [7/(2.4 + LVEDD) × LVEDD^3] − [7/(2.4 + LVESD) × LVESD^3] × 100 as described (43). The echocardiographer was blinded regarding the genotype of the animals.

RNA isolation and qRT–PCR

RNA isolation from heart and lung tissue as well as primary cardiac and pulmonary fibroblasts was performed as previously described (44). For qRT–PCR, cDNA was synthesized using Superscript II ReverseTranscriptase (Invitrogen, Germany) and Oligo(dT)$_{15}$ primer (Promega, Germany) according to the manufacturer's protocol. qRT–PCR was conducted using ABI Prims 7900HT Sequence Detection System and Power SYBR Green (Applied Biosystems, Germany). Determination of gene expression was performed as relative quantification and calculated as previously described (45,46).

Expression profiling

Genome-wide cDNA-chip-based expression profiling was performed with *Aga2*^{severe} animals at the age of 11 dpp. RNA samples from the heart and lung of three individual mutants were used and compared against a WT reference RNA pool from four littermate control mice.

cDNA microarrays were produced in-house and hybridized using a Cy3/Cy5 dual color approach as recently described (44). A full description of the probes on our microarray is available in the GEO database under GPL4937. Two independent dual color hybridizations including a dye-swap experiment were performed for each of the individual samples. Expression data of the analyzed *Aga2* heart and lung samples have been submitted to the GEO database (GSE12847).

Statistical analyses were performed using TM4 Microarray software suite including MIDAS (Microarray Data Analysis System) for normalization (47) and SAM (Significant Analysis of Microarrays) for the determination of genes showing significant differential regulation (48). The FDR was set to 0.5% for the heart and 0% for lung samples.

In silico analysis of differentially expressed genes was performed using EASE, a module of the DAVID database (44), assigning genes to GO functional categories. EASE analysis includes a Bonferroni multiplicity correlation and evaluates the set of differentially expressed genes for over-representation of biological processes. In-depth analysis and description of the denoted genes for molecular function and pathological involvements was additionally done using BiblioSphere Pathway Edition (Genomatix, Germany), including a comprehensive manual interpretation of the gene functions by intensive literature study.

Histology and SEM

Animals at the age of 11 and 10 days were used for histological studies and SEM analyses of heart and lung tissue, respectively. For histological analysis, embedding, staining for H&E and IHC were performed as previously described (24). Samples were analyzed using a Zeiss Axioplan2 fluorescent microscope equipped with the AxioVision 4.6.3.0 software and a Zeiss LSM510 confocal microscope with the corresponding program 3.2 SP2 (Zeiss, Germany).

For SEM of the heart, tissue was macerated, thereby preserving and exposing the remaining collagen structure and network (49). Specimens were critical-point-dried, coated with platinum and observed with a JEOL JSM 6300F SEM (JEOL, Japan).

In vitro cell culture

For *in vitro* analysis, primary heart and lung fibroblasts were isolated essentially previously described (50,51). Cells from single mice were cultured individually, or pooled by the phenotype (WT, *Aga2*^{mild}, *Aga2*^{severe}) and seeded with an initial density of 1×10^5 cells per well in a 24-well plate.

Experiments were performed between the first and third passages. After 48 h of incubation, ascorbic acid (50 µg/ml) was added and incubated for 24 h. For NMD experiments, cells were incubated for 16 h in the stimulation medium (ascorbic acid addition) and further 8 h in the stimulation medium containing emetine (100 µg/ml). Cultures were used for RNA isolation or immunocytochemistry (ICC) according to standard procedures.

Samples from ICC were observed under a Zeiss Axioplan2 fluorescent microscope equipped with AxioVision 4.6.3.0 software (Zeiss, Germany).

Chemicals and antibodies

Antibodies to Col1a1 (ab292) and PECAM (ab28364) were purchased from Abcam, UK. The fluorescent secondary antibodies Alexa Fluor 488 goat-anti-rabbit IgG were purchased from Abcam, UK, Alexa Fluor 594 donkey-anti-rabbit IgG from Molecular Probes and the Kit for DAB staining (Vectastain ABC kit) from Linaris, Germany.

Statistical analysis

All results are expressed as the means $\pm$ SEM of sample size n. In case $n \geq 3$, the statistical significance was tested by applying the non-parametric Mann–Whitney U-test using the StatView software package (SAS cooperation). P-values < 0.05 were considered significant with further subdivision: $^{*}P \leq 0.05$, $^{**}P \leq 0.01$, $^{***}P \leq 0.001$.

ACKNOWLEDGEMENTS

We would like to thank the members of the GMC for phenotyping of *Aga2* mice and fruitful discussions, the animal caretakers of the GMC for excellent and professional support, Nina Schieven, Michael Schulz, Helga Wehnes, Sandra Geißler, Reinhard Seeliger, Susanne Wittich and Miriam Backs for excellent technical assistance. We are grateful to the children and families of the NICHD longitudinal OI research population for their dedication to OI research and participation in our protocols. We thank the Nurses and staff of 1NW Clinical Unit at the NIH Clinical Center for care of our protocol patients.

Conflict of Interest statement. None declared.

FUNDING

This work was supported by the Nationales Genomforschungsnetzwerk (01GS0850 to M.H.A., 01GS0854 H.A.K.). The clinical trial was supported by funds from the National Institute of Child Health & Human Development Intramural Research Program. Funding to pay the Open Access publication charges for this article was provided by Helmholtz Zentrum München, German Research Center for Environmental Health (GmbH).

REFERENCES

1. Roughley, P.J., Rauch, F. and Glorieux, F.H. (2003) Osteogenesis imperfecta—clinical and molecular diversity. *Eur. Cell Mater.*, **5**, 41–47.
2. Marini, J.C., Cabral, W.A., Barnes, A.M. and Chang, W. (2007) Components of the collagen prolyl 3-hydroxylation complex are crucial for normal bone development. *Cell Cycle*, **6**, 1675–1681.
3. Barnes, A.M., Carter, E.M., Cabral, W.A., Weis, M., Chang, W., Makareeva, E., Leikin, S., Rotimi, C.N., Eyre, D.R., Raggio, C.L. *et al.* (9999) Lack of cyclophilin B in osteogenesis imperfecta with normal collagen folding. *N. Engl. J. Med.*, **362**, 521–528.
4. Rauch, F. and Glorieux, F.H. (2004) Osteogenesis imperfecta. *Lancet*, **363**, 1377–1385.
5. Martin, E. and Shapiro, J.R. (2007) Osteogenesis imperfecta: epidemiology and pathophysiology. *Curr. Osteoporos. Rep.*, **5**, 91–97.
6. Singer, R.B., Ogston, S.A. and Paterson, C.R. (2001) Mortality in various types of osteogenesis imperfecta. *J. Insur. Med.*, **33**, 216–220.
7. McAllion, S.J. and Paterson, C.R. (1996) Causes of death in osteogenesis imperfecta. *J. Clin. Pathol.*, **49**, 627–630.
8. Widmann, R.F., Bitan, F.D., Laplaza, F.J., Burke, S.W., DiMaio, M.F. and Schneider, R. (1999) Spinal deformity, pulmonary compromise, and quality of life in osteogenesis imperfecta. *Spine (Phila Pa 1976)*, **24**, 1673–1678.
9. Falvo, K.A., Klain, D.B., Krauss, A.N., Root, L. and Auld, P.A. (1973) Pulmonary function studies in osteogenesis imperfecta. *Am. Rev. Respir. Dis.*, **108**, 1258–1260.
10. Shapiro, J.R., Burn, V.E., Chipman, S.D., Jacobs, J.B., Schloo, B., Reid, L., Larsen, N. and Louis, F. (1989) Pulmonary hypoplasia and osteogenesis imperfecta type II with defective synthesis of alpha I(1) procollagen. *Bone*, **10**, 165–171.
11. Thibeault, D.W., Pettett, G., Mabry, S.M. and Rezaiekhaligh, M.M. (1995) Osteogenesis imperfecta type IIA and pulmonary hypoplasia with normal alveolar development. *Pediatr. Pulmonol.*, **20**, 301–306.
12. Hortop, J., Tsipouras, P., Hanley, J.A., Maron, B.J. and Shapiro, J.R. (1986) Cardiovascular involvement in osteogenesis imperfecta. *Circulation*, **73**, 54–61.
13. Vetter, U., Maierhofer, B., Muller, M., Lang, D., Teller, W.M., Brenner, R., Frohneberg, D. and Worsdorfer, O. (1989) Osteogenesis imperfecta in childhood: cardiac and renal manifestations. *Eur. J. Pediatr.*, **149**, 184–187.
14. Wong, R.S., Follis, F.M., Shively, B.K. and Wernly, J.A. (1995) Osteogenesis imperfecta and cardiovascular diseases. *Ann. Thorac. Surg.*, **60**, 1439–1443.
15. Moriyama, Y., Nishida, T., Toyohira, H., Saigenji, H., Shimokawa, S., Taira, A. and Kuriwaki, K. (1995) Acute aortic dissection in a patient with osteogenesis imperfecta. *Ann. Thorac. Surg.*, **60**, 1397–1399.
16. Zegdi, R., D'Attellis, N., Fornes, P., Fuzellier, J.F., Carteaux, J.P., Fabiani, J.N. and Carpentier, A. (1998) Aortic valve surgery in osteogenesis imperfecta: report of two cases and review of the literature. *J. Heart Valve Dis.*, **7**, 510–514.
17. Khashu, M., Pelligra, G., Sandor, G.G. and Singh, A.J. (2006) Right-sided cardiac involvement in osteogenesis imperfecta. *J. Heart Valve Dis.*, **15**, 588–590.
18. Isotalo, P.A., Guindi, M.M., Bedard, P., Brais, M.P. and Veinot, J.P. (1999) Aortic dissection: a rare complication of osteogenesis imperfecta. *Can. J. Cardiol.*, **15**, 1139–1142.
19. Bonita, R.E., Cohen, I.S. and Berko, B.A. (9999) Valvular heart disease in osteogenesis imperfecta: presentation of a case and review of the literature. *Echocardiography*, **27**, 69–73.
20. Weis, S.M., Emery, J.L., Becker, K.D., McBride, D.J. Jr, Omens, J.H. and McCulloch, A.D. (2000) Myocardial mechanics and collagen structure in the osteogenesis imperfecta murine (oim). *Circ. Res.*, **87**, 663–669.
21. Pfeiffer, B.J., Franklin, C.L., Hsieh, F.H., Bank, R.A. and Phillips, C.L. (2005) Alpha 2(I) collagen deficient oim mice have altered biomechanical integrity, collagen content, and collagen crosslinking of their thoracic aorta. *Matrix Biol.*, **24**, 451–458.
22. Wheeler, V.R., Cooley, N.R. Jr and Blackburn, W.R. (1988) Cardiovascular pathology in osteogenesis imperfecta type IIA with a review of the literature. *Pediatr. Pathol.*, **8**, 55–64.
23. Hrabe de Angelis, M.H., Flaswinkel, H., Fuchs, H., Rathkolb, B., Soewarto, D., Marschall, S., Heffner, S., Pargent, W., Wuensch, K., Jung, M. *et al.* (2000) Genome-wide, large-scale production of mutant mice by ENU mutagenesis. *Nat. Genet.*, **25**, 444–447.
24. Lisse, T.S., Thiele, F., Fuchs, H., Hans, W., Przemeck, G.K., Abe, K., Rathkolb, B., Quintanilla-Martinez, L., Hoelzlwimmer, G., Helfrich, M. *et al.* (2008) ER stress-mediated apoptosis in a new mouse model of osteogenesis imperfecta. *PLoS Genet.*, **4**, e7.
25. Schnieke, A., Harbers, K. and Jaenisch, R. (1983) Embryonic lethal mutation in mice induced by retrovirus insertion into the alpha 1(I) collagen gene. *Nature*, **304**, 315–320.
26. Butcher, H.L., Kennette, W.A., Collins, O., Zalups, R.K. and Koropatnick, J. (2004) Metallothionein mediates the level and activity of nuclear factor kappa B in murine fibroblasts. *J. Pharmacol. Exp. Ther.*, **310**, 589–598.
27. Novitskiy, G., Potter, J.J., Rennie-Tankersley, L. and Mezey, E. (2004) Identification of a novel NF-kappaB-binding site with regulation of the murine alpha2(I) collagen promoter. *J. Biol. Chem.*, **279**, 15639–15644.

28. Okamoto, O. and Fujiwara, S. (2006) Dermatopontin, a novel player in the biology of the extracellular matrix. *Connect. Tissue Res.*, **47**, 177–189.
29. Toyoshima, T., Ishida, T., Nishi, N., Kobayashi, R., Nakamura, T. and Itano, T. (2008) Differential gene expression of 36-kDa microfibril-associated glycoprotein (MAGP-36/MFAP4) in rat organs. *Cell Tissue Res.*, **332**, 271–278.
30. Janicki, J.S. and Brower, G.L. (2002) The role of myocardial fibrillar collagen in ventricular remodeling and function. *J. Card. Fail.*, **8**, S319–325.
31. Houweling, A.C., van Borren, M.M., Moorman, A.F. and Christoffels, V.M. (2005) Expression and regulation of the atrial natriuretic factor encoding gene Nppa during development and disease. *Cardiovasc. Res.*, **67**, 583–593.
32. Iwai, N., Shimoike, H. and Kinoshita, M. (1995) Genes up-regulated in hypertrophied ventricle. *Biochem. Biophys. Res. Commun.*, **209**, 527–534.
33. Walther, T., Tschope, C., Sterner-Kock, A., Westermann, D., Heringer-Walther, S., Riad, A., Nikolic, A., Wang, Y., Ebermann, L., Siems, W.E. *et al.* (2007) Accelerated mitochondrial adenosine diphosphate/adenosine triphosphate transport improves hypertension-induced heart disease. *Circulation*, **115**, 333–344.
34. Gao, X. and Xu, Z. (2008) Mechanisms of action of angiogenin. *Acta Biochim. Biophys. Sin. (Shanghai)*, **40**, 619–624.
35. Li, M. and Ransohoff, R.M. (2009) The roles of chemokine CXCL12 in embryonic and brain tumor angiogenesis. *Semin. Cancer Biol.*, **19**, 111–115.
36. Brigstock, D.R. (2002) Regulation of angiogenesis and endothelial cell function by connective tissue growth factor (CTGF) and cysteine-rich 61 (CYR61). *Angiogenesis*, **5**, 153–165.
37. Jones, P.L., Chapados, R., Baldwin, H.S., Raff, G.W., Vitvitsky, E.V., Spray, T.L. and Gaynor, J.W. (2002) Altered hemodynamics controls matrix metalloproteinase activity and tenascin-C expression in neonatal pig lung. *Am. J. Physiol. Lung Cell Mol. Physiol.*, **282**, L26–L35.
38. Migliaccio, S., Barbaro, G., Fornari, R., Di Lorenzo, G., Celli, M., Lubrano, C., Falcone, S., Fabbrini, E., Greco, E., Zambrano, A. *et al.* (2009) Impairment of diastolic function in adult patients affected by osteogenesis imperfecta clinically asymptomatic for cardiac disease: casuality or causality? *Int. J. Cardiol.*, **131**, 200–203.
39. Takken, T., Terlingen, H.C., Helders, P.J., Pruijs, H., Van der Ent, C.K. and Engelbert, R.H. (2004) Cardiopulmonary fitness and muscle strength in patients with osteogenesis imperfecta type I. *J. Pediatr.*, **145**, 813–818.
40. Gailus-Durner, V., Fuchs, H., Adler, T., Aguilar Pimentel, A., Becker, L., Bolle, I., Calzada-Wack, J., Dalke, C., Ehrhardt, N., Ferwagner, B. *et al.* (2009) Systemic first-line phenotyping. *Methods Mol. Biol.*, **530**, 1–47.
41. Gailus-Durner, V., Fuchs, H., Becker, L., Bolle, I., Brielmeier, M., Calzada-Wack, J., Elvert, R., Ehrhardt, N., Dalke, C., Franz, T.J. *et al.* (2005) Introducing the German Mouse Clinic: open access platform for standardized phenotyping. *Nat. Methods*, **2**, 403–404.
42. Sahn, D.J., DeMaria, A., Kisslo, J. and Weyman, A. (1978) Recommendations regarding quantitation in M-mode echocardiography: results of a survey of echocardiographic measurements. *Circulation*, **58**, 1072–1083.
43. Teichholz, L.E., Cohen, M.V., Sonnenblick, E.H. and Gorlin, R. (1974) Study of left ventricular geometry and function by B-scan ultrasonography in patients with and without asynergy. *N. Engl. J. Med.*, **291**, 1220–1226.
44. Horsch, M., Schadler, S., Gailus-Durner, V., Fuchs, H., Meyer, H., de Angelis, M.H. and Beckers, J. (2008) Systematic gene expression profiling of mouse model series reveals coexpressed genes. *Proteomics*, **8**, 1248–1256.
45. Pfaffl, M.W. (2001) A new mathematical model for relative quantification in real-time RT-PCR. *Nucleic Acids Res.*, **29**, e45.
46. Livak, K.J. and Schmittgen, T.D. (2001) Analysis of relative gene expression data using real-time quantitative PCR and the 2(-Delta Delta C(T)) Method. *Methods*, **25**, 402–408.
47. Quackenbush, J. (2002) Microarray data normalization and transformation. Nat. Genet., **32**(suppl.), 496–501.
48. Dennis, G. Jr, Sherman, B.T., Hosack, D.A., Yang, J., Gao, W., Lane, H.C. and Lempicki, R.A. (2003) DAVID: Database for Annotation, Visualization, and Integrated Discovery. *Genome Biol.*, **4**, P3.
49. Ohtani, O., Ushiki, T., Taguchi, T. and Kikuta, A. (1988) Collagen fibrillar networks as skeletal frameworks: a demonstration by cell-maceration/scanning electron microscope method. *Arch. Histol. Cytol.*, **51**, 249–261.
50. Eghbali, M., Tomek, R., Woods, C. and Bhambi, B. (1991) Cardiac fibroblasts are predisposed to convert into myocyte phenotype: specific effect of transforming growth factor beta. *Proc. Natl Acad. Sci. USA*, **88**, 795–799.
51. Phan, S.H., Varani, J. and Smith, D. (1985) Rat lung fibroblast collagen metabolism in bleomycin-induced pulmonary fibrosis. *J. Clin. Invest.*, **76**, 241–247.